2018 NDIA GROUND VEHICLE SYSTEMS ENGINEERING AND TECHNOLOGY SYMPOSIUM
MATERIALS & ADVANCE MANUFACTURING (M&AM) TECHNICAL SESSION
AUGUST 7-9, 2018 - NOVI, MICHIGAN

Modeling of Shear Thickening Fluids for Analysis of Energy Absorption Under Impulse Loading

Alyssa Bennett
Naval Architecture and Marine Engineering
University of Michigan
Ann Arbor, MI

Nickolas Vlahopoulos, PhD
Naval Architecture and Marine Engineering
University of Michigan
Ann Arbor, MI

Weiran Jiang, PhD
Research & Innovation Center
Ford Motor Company
Detroit, MI

Matthew Castanier, PhD
Ravi Thyagarajan, PhD
Scott Shurin
U.S. Army RDECOM-TARDEC
Warren, MI

ABSTRACT

A proposed new method of energy absorption in multilayered plates is to implement shear-thickening fluids between the plate layers to act as a damping mechanism. Research into the implementation of shear thickening fluids (STF) in Kevlar body armor has yielded positive results for ballistic loadings. The objective of this integrated computational materials engineering (ICME) study is to accurately model the behavior of shear thickening fluids using the discrete element method (DEM) to better understand shear-thickening mechanisms and how shear thickening fluids behave under high shear rates experienced during impulse loading. These results are implemented in a reduced order model of a multilayered plate to determine the effect of shear thickening fluids on energy absorption capabilities.

INTRODUCTION

Structural energy absorption is critical for improving vehicle survivability and mitigating occupant injury in blast events. Increasing armor material is not always a viable solution; the impact of vehicle weight on mission performance has become a major issue for military vehicles [1-3]. Implementing shear thickening fluids (STFs) between plate layers in multilayer plates to act as a damping mechanism may provide a solution to both these problems. Integrated computation materials engineering (ICME) provides a useful method for studying the behavior and implementation of new materials, such as STFs, in which reduced order models can easily be incorporated to link multiscale models [3,4].

Shear thickening is a non-Newtonian behavior where viscosity increases significantly, sometimes discontinuously, with shear rate [4-9]. This behavior of STFs has proven to be useful in a variety of defense applications. Impregnating Kevlar and other synthetic woven fabrics with an STF has improved body armor performance under ballistic loading conditions [10,11]. Furthermore, it has been proposed that STFs can be used to develop tuned dampers [12,13] and shock resistant batteries [14].

STFs are often colloidal suspensions consisting of densely packed, solid particles less than a micrometer in diameter [5-10, 14]. The causes of reversible shear thickening are thought to be hydroclusters, which are jamming clusters of particles caused by hydrodynamic lubrication forces between particles, and dilatancy, the expansion of the densely packed particles when they are subjected to large shear stresses[7,9].

The first section of this paper discusses the development of a preliminary micro-scale model of a STF developed in the CFD software STAR-CCM+. This model uses the discrete element method (DEM) to model the particles in the STF explicitly. The next section discusses a reduced order model used to capture the effects of implementing a STF at plate layer interfaces within a multilayer plate. The final section presents the results of these two models.

MICROSCALE MODEL OF STF

In this section, the methods used to develop the microscale model of the fluid phase and particles in the STF are discussed. The particles are modeled using the discrete element method (DEM) and are coupled with the fluid through drag and lubrication forces. The fluid is modeled using traditional finite volume CFD. Both the fluid phase and particles are modeled in the computational fluid dynamics program STAR-CCM+. Due to the computational demands of this model, HPC resources were used to run the simulations.

The STF used for this paper consists of silica particles 500 nanometers in diameter suspended in polyethylene glycol 200 (PEG 200) with a packing fraction of 0.57. The model is based on published measurements taken using a stress-controlled rheometer (SR-500, Rheometrics) with a 25 mm diameter cone and a cone angle of 0.1 radian [10]. The geometry of the cone and plate rheometer are shown in figure 1.

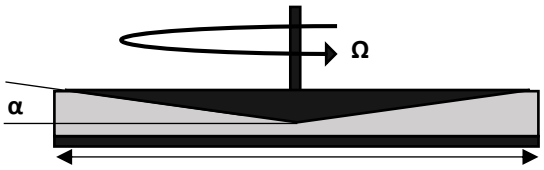

Figure 1: Geometry of cone and plate rheometer (fluid sample shown in grey)

Fluid Phase Modeling

Using the rheometer geometry, a three dimensional Eulerian mesh was generated in STAR CCM+. A no-slip wall boundary condition was applied to the top and bottom surfaces of the mesh to simulate the cone and plate of the rheometer. An atmospheric pressure boundary condition was applied to the outer edge of the fluid domain. All boundaries were given the additional condition that the particles could not pass through them. Figure 2 illustrates the application of the fluid boundary conditions.

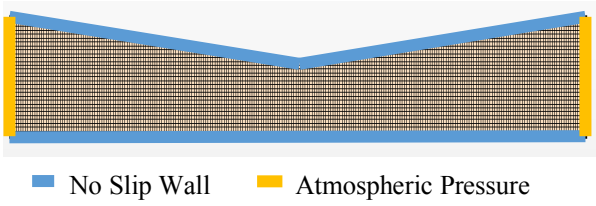

Figure 2: Boundary conditions applied to Eulerian Mesh

A rotational velocity was then applied to the top wall (the cone surface) to generate shear. Figure 3 shows the resulting velocity boundary condition along the top of the fluid domain for a local rotation

rate of 0.4 radians/second. A strain-controlled rather than stress-controlled boundary condition is used since the rheometer data is reported in terms of shear rate.

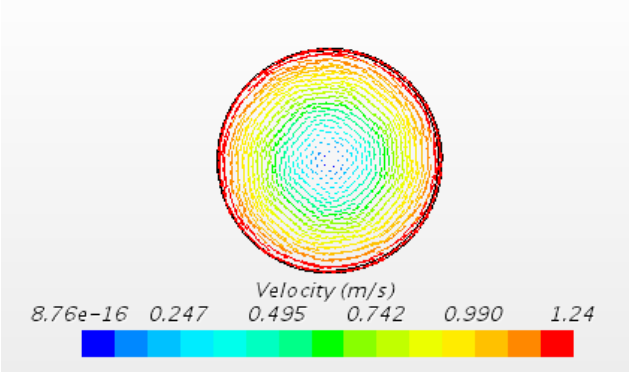

Figure 3: Example of top wall velocity boundary condition

In order to simulate conditions similar to those experienced under impulsive loads, the model was subjected to shear rates greater than 100 s^{-1}. The simulations were allowed to converge to a steady-state flow.

Particle Phase Modeling

The discrete element model (DEM) is used to model the behavior of the particles in the STF. DEM is a meshless, Lagrangian method that includes the particles' rotational degrees of freedom [15-19]. The particles are modeled as separate, spherical rigid bodies that interact with other particles and their environment through lateral and normal forces [15-19].

The forces acting on each particle in STAR-CCM+ are given in equations (1-2). F_d is the drag force acting on the particle, F_v is the viscous force that acts on the particle, and F_p is the force due to the pressure gradient that acts on the particle [17]. I is the moment of inertia of the particle and $\ddot{\theta}$ is the angular acceleration. The drag coefficients of the particles are calculated using Gidaspow's equation [17].

$$m_{particle}\frac{dv}{dt} = \boldsymbol{F}_d + \boldsymbol{F}_p + \boldsymbol{F}_{body} + \boldsymbol{F}_{contact} + \boldsymbol{F}_V \quad (1)$$

$$I\ddot{\theta} = r \times \boldsymbol{F}_{contact}^{tangental} \quad (2)$$

The Hertz-Mindlin contact model is used to calculate the contact force. The lubrication force between neighboring particles is proportional to their relative velocities, analogously to a damping force. The lubrication force acts along the normal vector between the two particle centroids and can be written in the general form:

$$\boldsymbol{F}_v^n = C_n \boldsymbol{v}_r^n \quad (3)$$

C_n is the damping coefficient related to the liquid viscosity as defined in Equation (4), where R is the particle radius, η_f is the dynamic viscosity of the fluid phase, and H is the initial distance between particles i and j as shown in figure 4 [18]. The relative velocity between particles i and j is $\boldsymbol{v}^n{}_r$, which is defined in Equation (5). To avoid singularity, the lubrication force is set to zero when H is equal to $0.01r$.

$$C_n = \frac{6\eta_f \pi R^2}{H} \quad (4)$$

$$\boldsymbol{v}_r^n = \left((\boldsymbol{v}_i - \boldsymbol{v}_j)\cdot \boldsymbol{n}\right)\boldsymbol{n} \quad (5)$$

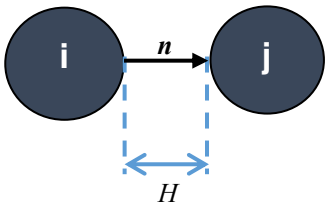

Figure 4: Two DEM particles distance H away from each other

The effects of the particle motion on the fluid phase appear as a source term in the momentum equation for each Eulerian cell. This source term, defined in Equation (6), is calculated by summing the integral of the drag force and mass flow rate of each particle in the cell over its time of residency and then dividing by the time step [17].

$$S = -\left(\frac{1}{\Delta t}\right)\sum_i \int_0^{\delta t}\left(\boldsymbol{F}_{drag} + \dot{m}_i \boldsymbol{v}\right)\delta t \quad (6)$$

The particles are randomly injected into the fluid domain and allowed to settle before the velocity boundary condition is applied.

Calculating Viscosity

Equation (7) gives the general relationship between shear stress, τ, effective fluid dynamic viscosity, η, and shear rate, $\dot{\gamma}$.

$$\tau = \eta\dot{\gamma} \tag{7}$$

The shear rate for a cone and plate rheometer with cone angle, α, less than or equal to 0.1 radians is given in Equation (8) [8]. Ω is the rotational speed in rad s^{-1} at which the cone turns.

$$\dot{\gamma}(r) \cong \frac{\Omega}{\alpha} \tag{8}$$

The shear stress is calculated using the measured torque on the cone, *T*. Equation (9) gives the relationship between the shear stress at the edge of the cone, $\tau(R)$, and *T*[8]. R_C is the radius of the cone itself.

$$\tau = \frac{3T}{2\pi R_c^3} \tag{9}$$

REDUCED ORDER MODEL OF MULTILAYER PLATE

In this section, the steps necessary to develop a reduced order model of a multilayer plate with the STF implemented along the layer interfaces using the reverberation matrix method (RMM) are described. RMM is used due to its capability to accurately model the dynamic response of multilayer plates in the frequency domain and the simplicity of implementing boundary effects at the layer interfaces to the model [19-22]. The steps to develop the RMM model are: defining the local coordinates and interface boundary conditions, defining the propagation of shear and pressure waves in the frequency domain, and finally defining the reverberation matrix itself. This model is used as a macro-scale model of the multilayer plates and shear thickening fluid.

Coordinate Definition

The N-layer multilayer plate is assumed wide enough that boundary conditions do not affect its response, meaning that the plate is modeled as infinitely wide. A two dimensional coordinate system (x,z) is defined at the 0^{th} interface in the same plane as the shear and pressure wave normals. Local coordinates are defined at each layer interface, as shown in figure 5.

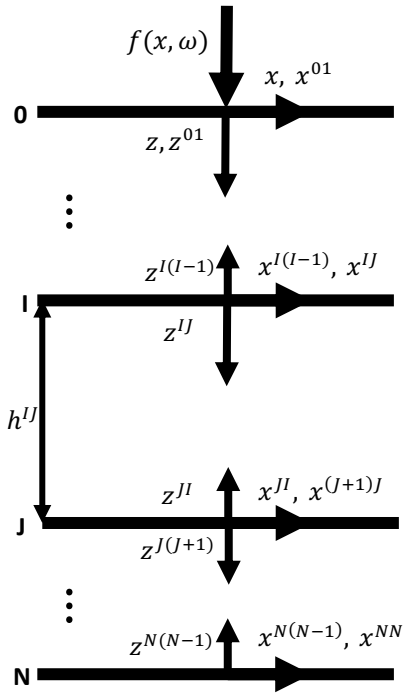

Figure 5: Local coordinates for an infinitely wide plate

The material properties of each J^{th} layer are isotropic. The force applied at each interface is defined as a vector $\mathbf{f^J}$.

Wave Propagation in Frequency Domain

The reverberation matrix method uses shear and pressure waves to determine the dynamic response of the multilayer plate. A double Fourier Transform is performed on the fundamental equations for shear and pressure waves to transfer them from the time and space domains to the frequency ω and wave number *k* domains. Equations (10a) and (10b)

give the resulting general wave equations for the pressure wave (p-wave) and shear wave (sv-wave) respectively, where is the transformed pressure wave potential and is the transformed shear wave potential.

$$\frac{d^2\tilde{\varphi}}{dz^2} + \alpha^2\tilde{\varphi} = 0 \qquad (10a)$$

$$\frac{d^2\tilde{\psi}}{dz^2} + \beta^2\tilde{\psi} = 0 \qquad (10b)$$

The p-wave and s-wave numbers in the z-direction are given by equations (11 a-b) respectively. C_p is the p-wave speed, and C_s is sv-wave speed.

$$\alpha = \sqrt{\frac{\omega^2}{C_p^2} - k^2} \qquad (11a)$$

$$\beta = \sqrt{\frac{\omega^2}{C_s^2} - k^2} \qquad (11b)$$

The general solutions for the wave equations can be described in terms of the unknown arrival wave amplitudes, $\tilde{a}_p$ and $\tilde{a}_s$, and the unknown departure wave amplitudes, $\tilde{d}_p$ and $\tilde{d}_s$, at the interface. These solutions are as follows:

$$\tilde{\varphi}(k,z,\omega) = \tilde{a}_p(k,w)e^{-i\alpha z} + \tilde{d}_p(k,w)e^{i\alpha z} \quad (11a)$$

$$\tilde{\psi}(k,z,\omega) = \tilde{a}_s(k,w)e^{-i\alpha z} + \tilde{d}_s(k,w)e^{i\alpha z} \quad (11b)$$

The displacements and stress components in the x-z plane are determined by applying the fundamental elastodynamic solutions.

Interface Boundary Conditions and Implementation of Shear Thickening Fluid

At each J[th] interface, the plate layers have equal and opposite traction forces applied to them to maintain equilibrium. For fully bonded interfaces, the plate layers at the interface have the same displacements. These conditions yield the boundary conditions described in equations (12 a-d). The superscripts *(J-1)* and (J+1) indicate if the displacement or stress is measured on the upper or lower side of the interface respectively.

$$u_x^{J(J-1)} - u_x^{J(J+1)} = 0 \qquad (12a)$$

$$u_z^{J(J-1)} + u_z^{J(J+1)} = 0 \qquad (12b)$$

$$\sigma_{xz}^{J(J-1)} + \sigma_{xz}^{J(J+1)} = 0 \qquad (12c)$$

$$\sigma_{zz}^{J(J-1)} - \sigma_{zz}^{J(J+1)} = 0 \qquad (12d)$$

The bottom face of the plate is assumed to be traction free, while the only traction acting on the top of the plate is the vector **f**(ω). Therefore there are only two boundary conditions at the *0* and *N* interfaces of the plate.

When the STF is placed at the layer interfaces lateral sliding occurs, meaning that the boundary condition given in Equation (12a) is no longer valid. Instead, a traction proportional to the relative lateral velocity of the plate layers occurs which is analogous to adding a damping force along the layer interface. This new boundary condition is given by Equation (13).

$$C_{eq}(\dot{u}_x^{J(J-1)} - \dot{u}_x^{J(J+1)}) = -\sigma_{xz}^{J(J-1)} \qquad (13)$$

This coefficient is calculated using the definition of work. The work done by a viscous damper over a complete period of vibration is given by equations (14 a-b), in which X is the amplitude of vibration and ω is the angular frequency of vibration [23].

$$W = \oint C_{eq}\dot{u}_x dx = \int_0^{\frac{2\pi}{\omega}} C_{eq}\dot{u}_x^2 dt \qquad (14a)$$

$$W = -\pi C_{eq}\omega X^2 \qquad (14b)$$

The work necessary to shear a fluid between two parallel plates is given by Equation (15). τ is the shear stress acting on the fluid across the surface area *A* and η is the fluid's effective dynamic viscosity. Using the definition of shear for a Couette flow between two parallel plates separated by a gap of height *h,* given in Equation (16), the

equivalent damping coefficient for a Newtonian fluid is given by Equation (17)[23].

$$W = \oint \tau dx = \oint \eta \dot{\gamma} dx = \int_0^{\frac{2\pi}{\omega}} \eta \frac{\partial \dot{u}_x}{\partial z} \dot{u}_x dt \quad (15)$$

$$\frac{\partial \dot{u}_x}{\partial z} = \frac{i\omega X}{h} \quad (16)$$

$$C_{eq} = \frac{\eta}{h} \quad (17)$$

For a non-Newtonian fluid, η is not a constant, but rather is a function of shear rate. This relationship can be calculated from the results of the previously discussed microscale model.

Reverberation Matrix Definition

By inserting the elastodynamic solutions into the boundary conditions, a linear system is built to describe the scattering phenomena at each J[th] interface in terms of the unknown arriving wave amplitudes and departing wave amplitudes at the interface. Equations (18 a-b) describe these vectors respectively.

$$\tilde{\boldsymbol{a}}^{\boldsymbol{J}} = \left[\tilde{a}_p^{J(J-1)}, \tilde{a}_s^{J(J-1)}, \tilde{a}_p^{J(J+1)}, \tilde{a}_s^{J(J+1)}\right] \quad (18a)$$

$$\tilde{\boldsymbol{d}}^{\boldsymbol{J}} = \left[\tilde{d}_p^{J(J-1)}, \tilde{d}_s^{J(J-1)}, \tilde{d}_p^{J(J+1)}, \tilde{d}_s^{J(J+1)}\right] \quad (18b)$$

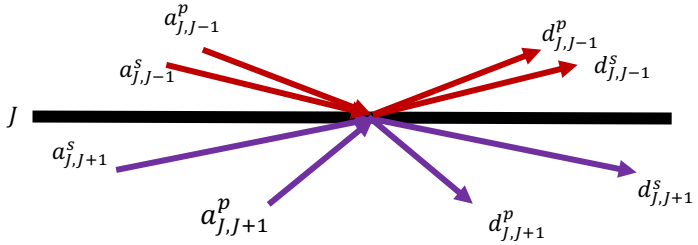

Figure 6: Arriving and departing waves at interface *J*

This system is then written as Equation (19) where S[J] is the local 4x4 scattering matrix at interface J and s[J] is the local 4x1 source vector at interface J that corresponds to the right hand side of the boundary conditions.

$$\tilde{\boldsymbol{d}}^{\boldsymbol{J}} = \boldsymbol{S}^{\boldsymbol{J}} \tilde{\boldsymbol{a}}^{\boldsymbol{J}} + \tilde{\boldsymbol{s}}^{\boldsymbol{J}} \quad (19)$$

At the top and bottom faces of the plate, the scattering matrix collapses into a 2x2 matrix due to the boundary conditions and the presence of only one plate layer along these surfaces. The global scattering matrix for the entire plate is described by Equation (20).

$$\begin{bmatrix} \tilde{\boldsymbol{d}}^{\boldsymbol{0}} \\ \tilde{\boldsymbol{d}}^{\boldsymbol{1}} \\ \vdots \\ \tilde{\boldsymbol{d}}^{\boldsymbol{N-1}} \\ \tilde{\boldsymbol{d}}^{\boldsymbol{N}} \end{bmatrix} = \begin{bmatrix} \boldsymbol{S}^{\boldsymbol{0}} & 0 & \cdots & 0 & 0 \\ 0 & \boldsymbol{S}^{\boldsymbol{1}} & & 0 & 0 \\ \vdots & & \ddots & \vdots & \\ 0 & 0 & \cdots & \boldsymbol{S}^{\boldsymbol{N-1}} & 0 \\ 0 & 0 & \cdots & 0 & \boldsymbol{S}^{\boldsymbol{N}} \end{bmatrix} \begin{bmatrix} \tilde{\boldsymbol{a}}^{\boldsymbol{0}} \\ \tilde{\boldsymbol{a}}^{\boldsymbol{1}} \\ \vdots \\ \tilde{\boldsymbol{a}}^{\boldsymbol{N-1}} \\ \tilde{\boldsymbol{a}}^{\boldsymbol{N}} \end{bmatrix} + \begin{bmatrix} \tilde{\boldsymbol{s}}^{\boldsymbol{0}} \\ \tilde{\boldsymbol{s}}^{\boldsymbol{1}} \\ \vdots \\ \tilde{\boldsymbol{s}}^{\boldsymbol{N-1}} \\ \tilde{\boldsymbol{s}}^{\boldsymbol{N}} \end{bmatrix} \quad (20)$$

The waves that depart from an interface on one side of the plate layer become the arriving waves at the other side of the plate layer with a phase lag. Similarly, all arrival and departure waves within a plate layer can be linked using a 4Nx4N phase matrix **P**(h) by Equation (21). Equations (22 a-b) describe **P**(h).

$$\tilde{\boldsymbol{a}} = \boldsymbol{P}(h)\tilde{\boldsymbol{d}}^* \quad (21)$$

$$\boldsymbol{P_J}(h_J) = \begin{bmatrix} e^{i\alpha_J h_J} & 0 \\ 0 & e^{i\beta_J h_J} \end{bmatrix} \quad (22\text{ a})$$

$$\boldsymbol{P} = \begin{bmatrix} \boldsymbol{P_1}(h_1) & 0 & \cdots & 0 \\ 0 & \boldsymbol{P_1}(h_1) & & \vdots \\ \vdots & & \boldsymbol{P_N}(h_N) & 0 \\ 0 & \cdots & 0 & \boldsymbol{P_N}(h_N) \end{bmatrix} \quad (22b)$$

The elements in $\tilde{\boldsymbol{d}}^*$ and $\tilde{\boldsymbol{d}}$ for each layer are the same and are linked through Equation (23), where **u** is the local permutation matrix. Equation (24) describes the local and global permutation matrices.

$$\tilde{\boldsymbol{d}}^* = \boldsymbol{u}\tilde{\boldsymbol{d}} \quad (23)$$

$$\boldsymbol{U} = \begin{bmatrix} \boldsymbol{u} & \cdots & 0 \\ \vdots & \ddots & \vdots \\ 0 & \cdots & \boldsymbol{u} \end{bmatrix}, \ \boldsymbol{u} = \begin{bmatrix} 0 & 0 & 1 & 0 \\ 0 & 0 & 0 & 1 \\ 1 & 0 & 0 & 0 \\ 0 & 1 & 0 & 0 \end{bmatrix} \quad (24)$$

The reverberation matrix, **R**, is defined as the product of the scattering, phase, and permutation matrices. Equations (26 a-b) state the relationship

between **R** and the arriving and departing wave amplitudes.

$$\boldsymbol{R}(k,\omega) = \boldsymbol{SPU} \quad (25)$$

$$\tilde{\boldsymbol{a}} = \boldsymbol{PU}[\boldsymbol{I} - \boldsymbol{R}]^{-1}\tilde{\boldsymbol{s}} \quad (26a)$$

$$\tilde{\boldsymbol{d}} = [\boldsymbol{I} - \boldsymbol{R}]^{-1}\tilde{\boldsymbol{s}} \quad (26b)$$

Dynamic Response

The dynamic response of the plate ,$\boldsymbol{G}$, is defined in Equation (27). $\boldsymbol{A_u}$ and $\boldsymbol{D_u}$ are the receiving matrices and are The Nuemann series is used to calculate the inverse of [I-R], as shown in Equation (29). An inverse Fourier Transform is performed on the dynamic response with respect to the wave number to return it to the frequency, displacement domain.

$$\boldsymbol{G}(k,z,\omega) = A_u\tilde{\boldsymbol{a}} + D_u\tilde{\boldsymbol{d}} = (A_u PU + D_u)[I - R]^{-1}\tilde{\boldsymbol{s}} \quad (27)$$

$$[\boldsymbol{I} - \boldsymbol{R}]^{-1} = \boldsymbol{I} + \boldsymbol{R} + \boldsymbol{R}^2 + \boldsymbol{R}^3 + \cdots + \boldsymbol{R}^M \quad (28)$$

Results

STAR-CCM+

The comparison between the STAR-CCM+ simulation results and the published rheometer data are shown in figure 7. As shown in this figure, initial simulations that did not include the lubrication forces between the particles resulted in significantly lower effective viscosities. However, implementing the lubrication forces lead to a large increase in the model's accuracy. This behavior agrees with previous findings on the behavior of STFs, which emphasize the importance of lubrication forces in shear-thickening behavior [5,6]. Dilatancy did occur in the simulations, as shown in figure 8.

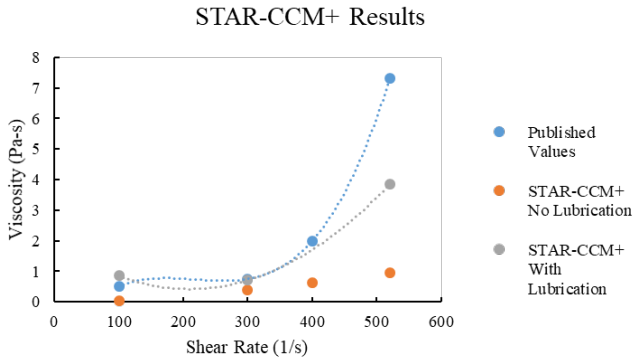

Figure 7: STAR-CCM+ results plotted against measured values

The polynomial relationship between the shear rate and effective viscosity is calculated using least squares, yielding Equation (29).

$$\eta = 1.992 - 0.0015\dot{\gamma} + 4 * 10^{-5}(\dot{\gamma})^2 \quad (29)$$

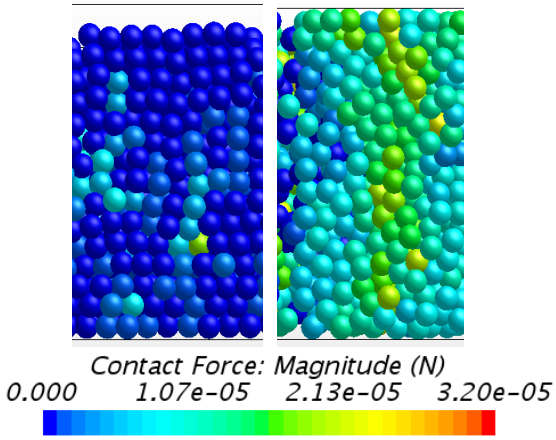

Figure 8: Initial particle position (left) and particle positions at steady state shear (right); increase in contact force between particles is shown

While the effective viscosities measured using the STAR-CCM+ model agree with published values at lower shear rates, the model does not accurately capture the shear thickening properties of the fluid at higher shear rates. This may indicate a need for a more complex model of lubrication forces between the particles at these shear rates.

Reduced Order Model of Multilayer Plate

To implement the behavior of the STF, the viscosity term in Equation (17) was replaced with Equation (29). An iterative method is used to solve for the dynamic response at each layer interface due to the non-linear dependency of the STF viscosity on shear rate. A five layer plate is simulated; each layer is 0.02 meters thick and made of steel. A unit load is applied to the bottom side of the plate.

Figure 9 shows the vertical dynamic response of the plate divided by its corresponding input power.

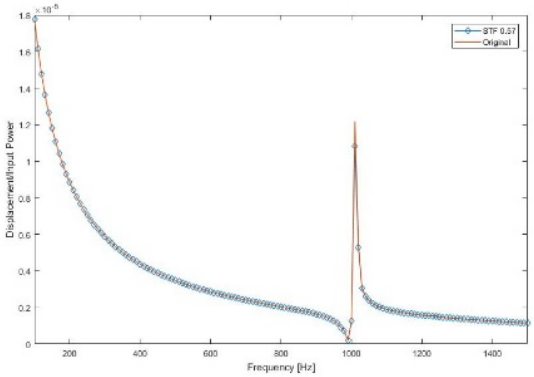

Figure 9: Vertical dynamic response divided by input power for multilayer plate with and without STF at layer interfaces

Implementing the effects of the STF mainly affected the plate's dynamic response at around peak response frequencies. This corresponds to the fact that the shear rate between plate layers is greatest at these frequencies.

CONCLUSIONS

In this paper a method of modeling STFs on the microscale using the discrete element method in STAR-CCM+ is presented. This paper also discusses using the reverberation matrix method to develop a reduced order, macroscale model of STFs for structural analysis.

The following conclusions are drawn:

- The results from the microscale STAR-CCM+ simulations indicate the importance of lubrication forces in modeling the shear thickening behavior of STFs.
- The macroscale, RMM model is able to incorporate the viscosity of the STF along the interfaces of a multilayer plate and showed that implementing STFs into multilayer plates reduces their dynamic response.
- STFs may provide a unique energy absorption mechanism for multilayer plates used in vehicle armor.

While the presented model results are promising, future work includes:

- Developing an improved model of the particle lubrication forces to improve the microscale model accuracy, especially for shear rates greater than 300 s^{-1}
- Implementing high pressure loading conditions to the microscale STAR-CCM+ model to study its effect on the model's results

Reference herein to any specific commercial company, product, process, or service by trade name, trademark, manufacturer, or otherwise does not necessarily constitute or imply its endorsement, recommendation, or favoring by the United States Government or the Department of the Army (DoA). The opinions of the authors expressed herein do not necessarily state or reflect those of the United States Government or the DoA and shall not be used for advertising or product endorsement purposes.

REFERENCES

[1]"Lightweight Combat Vehicle S&T Campaign, Project Final Technical Report", TARDEC Tech Report No 25940, October 2014

[2] Jiang, W., Vlahopoulos, N., Castanier, M. P., Thyagarajan, R., Mohammad, S., "Reducing Structural Weight and Increasing Protection in Simple Structures Subjected to Blast Loads", NDIA Ground Vehicle Systems Engineering And Technology Symposium, Aug, 2014

[3] Jiang, W., Vlahopoulos, N., Castanier, M.P., Thyagarajan, R,. Mohammad, S., "Tuning material and component properties to reduce weight and increase blastworthiness of a notional V-hull structure," Journal of Case Studies in Mechanical Systems and Signal Processing, 2, 2015

[4] Joost, W.J., "Reducing Vehicle Weight and Improving U.S. Energy Efficiency Using Integrated Computational Materials

Engineering", Journal of Materials, 64, pages 1032-1038, 2012

[5]S. Gurgen, L. Wiehua, M. Kushan, "The rheology of shear thickening fluids with various ceramic particle additives", Materials and Design, 104, pages 312-319, 2016

[6] E. Brown, H. Jaeger, "Shear thickening in concentrated suspensions: phenomenology, mechanisms and relations to jamming", Reports on Progress in Physics, 77, 2014

[7] H Barnes, "Shear thickening "Dilatancy" in suspensions of nonaggregating solid particles dispersed in Newtonian liquids", Journal of Rheology, 33, pages 329-363, 1989

[8] Mewis, J., Wagner, N., "Colloidal Suspension Rheology", Cambridge University Press, 2012

[9] R. Seto, R. Mari, J. Morris, M. Denn, "Discontinuous Shear Thickening of Frictional Hard-Sphere Suspensions", American Physical Society, November 2013

[10] Y.S. Lee, E Wetzel, N. Wagner, "The ballistic impact characteristics of Kevlar woven fabrics impregnated with a colloidal shear thickening fluid", Journal of Materials Science, 38, pages 2825-2833, 2003

[11] N. Asiga, H. Chouhan, S. Gebremeskel, N. Bhatnagar, "Impact Response of Shear Thickening fluid (STF) Treated High Strength Polymer Composites – Effect of STF Intercalation Method", 11th International Symposium on Plasticity and Impact Mechanics, 2016

[12] F. Yeh, K. Chang, T. Chen, "Smart Viscous Dampers utilizing Shear Thickening Fluids with Silica Nanoparticles", 15th World Conference on Earthquake Engineering, 2012

[13] XZ Zhang, WH Li, "The rheology of shear thickening fluid (STF) and the dynamic performance of an STF-filled damper", Smart Materials and Structures, 17, April 2008

[14]G. Veith, "Shear Thickening Electrolytes for High Impact Resistant Batteries", ACS Energy Letters, Vol 2 Issue 9, pages 2084-2088, 2017

[15] S. Luding, "Introduction to Discrete Element Methods", Multiscale Mechanics, pages 785-826, 2008

[16] K. Mishara, R. Rajamani, "The discrete element method for the simulation of ball mills", Applied Mathematical Modelling, Vol 16 Issue 11, Pages 598-604, 1992

[17] STAR-CCM+, "Theory Manual", Version: 12.04.010, 2017

[18] A. Vazquez-Quesada, M. Ellero, "Analytical solution for the lubrication force between two sphere in a bi-viscous fluid", Physics of Fluids, 28, 2016

[19] J. Weiran, A. Bennett, N. Vlahopoulos, M. Castanier, R. Thyagarajan, "A Reduced-Order Model for Evaluating the Dynamic Response of Multilayer Plates to Impulsive Loads", SAE International Journal Passenger Cars, 9, pages 83-89, 2016

[20]X. Su, J. Tian, Y. Pao, "Application of the reverberation-ray matrix to the propagation of elastic waves in layered solid", International Journal of Solids and Structures, 39, 5447-5463, 2002

[21] W. Yan, J. Wang, W. Chen, "Delamination assessment of a laminated composite beam using distributed piezoelectric sensor/actuator", Smart Materials and Structures, 20, 2011

[22] Chen, W.Q., Wang. H.M. Bao, R.H, "On calculating dispersion curves of waves in a functionally graded elastic plate," Composite Strucutres, Volume 81, Issue 2, 2007

[23] M.D. Symans and M.C. Constantinou, "Passive Fluid Viscous Damping Systems for Seismic Energy Dissipation" , ISTE Journal of Earthquake Technology, Vol 35, No 4, pages 185-206, 1998